J. Fluid Mech. (2012), *vol.* 691, *pp.* 1–25. © Cambridge University Press 2011
doi:10.1017/jfm.2011.436

Nonlinear interactions between deep-water waves and currents

R. M. Moreira† and D. H. Peregrine‡

School of Mathematics, University of Bristol, University Walk, Bristol BS8 1TW, UK

(Received 22 February 2011; revised 6 September 2011; accepted 3 October 2011;
first published online 6 December 2011)

The effects of nonlinearity on a train of linear water waves in deep water interacting with underlying currents are investigated numerically via a boundary-integral method. The current is assumed to be two-dimensional and stationary, being induced by a distribution of singularities located beneath the free surface, which impose sharp and gentle surface velocity gradients. For 'slowly' varying currents, the fully nonlinear results confirm that opposing currents induce wave steepening and breaking within the region where a high convergence of rays occurs. For 'rapidly' varying currents, wave blocking and breaking are more prominent. In this case reflection was observed when sufficiently strong adverse currents are imposed, confirming that at least part of the wave energy that builds up within the caustic can be released in the form of partial reflection and wave breaking. For bichromatic waves, the fully nonlinear results show that partial wave blocking occurs at the individual wave components in the wave groups and that waves become almost monochromatic upstream of the blocking region.

Key words: surface gravity waves, wave breaking, waves/free-surface flows

1. Introduction

Wave–current interactions occur in nature over a wide range of hydrodynamic length scales. Giant waves have been registered in some parts of the world, especially off the east coast of South Africa, where long waves are focused by the Agulhas current (Mallory 1974; Kharif & Pelinovsky 2006). Short surface waves propagating into a strong enough opposing current can be blocked such as at the entrances of tidal inlets (Vincent 1979; Battjes 1982). In both cases the adverse current augments the wave height and steepness, resulting in increased breaking and thus adding to the hazards of navigation. The varied physical circumstances in which these interactions occur and the different mathematical approaches that are applicable to them can be found in the review papers of Peregrine (1976), Jonsson (1990) and Thomas & Klopman (1997).

A particular area of interest is the interaction between short-scale gravity waves and strong large-scale currents. In this case the time and length scales over which the current varies are much larger than the wave period or wavelength. If these waves

† Present address: Computational Fluid Dynamics Laboratory, Fluminense Federal University, Rua Passo da Pátria 156, bl.D, sl.563A, Niterói, RJ 24210-240, Brazil. Email address for correspondence: roger@vm.uff.br

‡ Professor Peregrine passed away before this paper was completed. This manuscript was prepared for publication by the first author.

https://doi.org/10.1017/jfm.2011.436 Published online by Cambridge University Press

propagate into a strong enough opposing current, then their group velocity could be reduced to zero causing the waves to be blocked. A region almost free of wave activity is formed upstream from the blocking point while a strong increase in wave steepness is observed downstream, leading to rough water surfaces. Short surface waves propagating over a steady but non-uniform current tend to undergo refractive changes in length, direction and amplitude. Under certain conditions a simple linear ray theory can predict these properties accurately. The changes in length and direction depend on kinematical considerations only; however, changes in the wave amplitude are less straightforward. Wave amplitudes become essentially nonlinear at the blocking point and therefore the linear solutions are no longer accurate.

Thus the study of wave–current interactions has been a topic of active research among scientists for many years, with several theoretical approaches (Longuet-Higgins & Stewart 1960, 1961; Bretherton & Garrett 1968; Crapper 1972; Smith 1975; Peregrine & Smith 1979; Peregrine & Thomas 1979; Stiassnie & Dagan 1979). Recently direct modelling of wave blocking has been done with the help of Boussinesq models (Chen *et al.* 1998; Chawla 1999), which have the advantage of being nonlinear and thus can be used to study amplitude dispersion and energy transfer effects in the dynamics of wave blocking. However, for short waves the dispersive properties are not very well predicted, with the discrepancies in the dispersion relation leading to significant errors in the wave blocking region. The complexity of the wave field and the theoretical difficulties in understanding the dynamics near the blocking point stimulated several researchers to carry out experimental work in this field (Sakai & Saeki 1984; Lai, Long & Huang 1989; Ris & Holthuijsen 1996; Chawla & Kirby 1998; Suastika, de Jong & Battjes 2000; Chawla & Kirby 2002).

Though there are several theoretical and experimental works on waves propagating against adverse currents, few fully nonlinear numerical models considering both incident and reflected waves in the blocking region can be found in the literature. Peregrine & Thomas (1979) suggested that solutions involving both types of waves needed to be considered in the analysis in order to solve these caustic problems. The current work aims to study via fully nonlinear computations the behaviour of a train of linear water waves in deep water when meeting non-uniform currents, especially in the region where linear solutions become singular. In particular 'rapidly' varying surface currents are imposed in order to verify the wave transformation that occurs at the blocking region. It is shown that wave blocking and breaking are more prominent than in the solutions found for a gentle surface current and that reflection occurs when sufficiently strong adverse currents are imposed. The computed incident, reflected and transmitted waves are compared to linear theory, with wavelengths found to agree rather well, but not wave amplitudes. The numerical simulations can help to clarify some aspects of the nonlinear interaction such as the extension of the concept of group velocity to nonlinear waves and the prediction of surface wave properties in the region where linear ray theory breaks down.

2. Governing equations

2.1. *Unsteady nonlinear model*

In order to simulate the nonlinear evolution of periodic surface waves on a current, an underlying flow is modelled via a stationary distribution of singularities underneath the free surface. Basically the concept of introducing a single singular point in a non-periodic domain (such as used by Moreira & Peregrine 2010) is extended in order to generate spatially periodic free-surface flows with gentle and sharp current

https://doi.org/10.1017/jfm.2011.436 Published online by Cambridge University Press

gradients. The method of solution consists of applying a boundary-integral method to a free-surface flow problem, which reduces significantly the computational demand for the calculation of the fluid motion since only surface properties are evaluated (Dold & Peregrine 1986; Dold 1992). The solution is based on solving an integral equation that arises from Cauchy's integral theorem for functions of a complex variable.

The fluid flow is assumed to be inviscid and incompressible with the singularities distributed below the free surface at fixed points $\boldsymbol{x}_{s_i}$. It is also assumed that the flow is irrotational outside the singular cores and away from the free surface. The irrotational velocity field $\boldsymbol{u}(x, y, t)$ is then given by the gradient of a velocity potential $\Phi(x, y, t)$ which satisfies Laplace's equation in the fluid domain, excluding the singular points. The coordinate axes, x and y, have their origin located at the undisturbed level of the free surface. All the interior properties of the fluid are then determined by its properties at the boundaries alone. The entire motion can be modelled by considering a point discretisation of the surface.

To apply Cauchy's integral theorem to the problem, the potential Φ must be known on all the boundaries. The kinematic and dynamic boundary conditions are applied at the free surface such that

$$\frac{\mathrm{D}\boldsymbol{r}}{\mathrm{D}t} = \nabla\Phi, \quad \frac{\mathrm{D}\Phi}{\mathrm{D}t} = \frac{1}{2}|\nabla\Phi|^2 - gy - \frac{p}{\rho}, \tag{2.1}$$

where $\boldsymbol{r} = (x, y, t)$; $y = \eta(x, t)$ is the elevation of the free surface above the undisturbed water level; g is the acceleration due to gravity; and ρ is the fluid density. The pressure p exerted on the exterior side of the surface can be chosen to approximate the effects of wind, capillarity or a localised pressure on the surface, though for simplicity it is not used in the present calculations.

Attention is directed to the case where a periodic train of short waves with initially uniform wavenumber interacts with an underlying current. A strong gust of wind over the sea surface may generate a periodic set of short waves of initially approximately uniform wavenumber. It is convenient to assume that the wave surface is periodic in x, not only for the purpose of computing a numerical solution, but also to guarantee that the solution surface looks like a periodic plane wave train, satisfying linear ray theory assumptions and also avoiding more complicated wave patterns. This is particularly important for validation of the numerical results. Authors who have similarly employed spatially periodic domains to study other related wave–current problems include Donato, Peregrine & Stocker (1999) and Stocker & Peregrine (1999).

The velocity potential $\Phi(x, y, t)$ and the velocity $\boldsymbol{u}(x, y, t)$ are then required to be continuous at the vertical boundaries such that

$$\nabla\Phi(0, y, t) = \nabla\Phi(2\pi, y, t), \tag{2.2}$$

valid for $-\infty < y \leqslant 0$ and $t > 0$. Here the length units are chosen to make the period equal to 2π, which is convenient for a periodic domain. It is also assumed that the water is deep, satisfying the condition $|\nabla\Phi| \to 0$ as $y \to -\infty$. To complete the model, an initial condition for the free surface is required such that $\eta(x, t) = \eta_0(x, 0)$ and $\Phi(x, \eta, t) = \Phi_0(x, \eta_0, 0)$, as will be defined in § 2.3. To characterise the fluid motion in deep water, the Froude number is defined as

$$Fr = \frac{\gamma}{\sqrt{gd^3}}, \tag{2.3}$$

where γ and d are the strength and the depth of submergence of the singularities.

https://doi.org/10.1017/jfm.2011.436 Published online by Cambridge University Press

2.2. *Free-surface currents induced by singularities*

The use of singularities in the modelling of free-surface flows has been a common tool for researchers for many years in order to understand the basics and complexities of several natural phenomena. Lamb (1932) was perhaps the first to register the value of singularities when modelling free-surface flows, helping to disseminate this concept. Singularities have become widely employed in fluid mechanics, whether in the investigation of nonlinear effects at the free surface due to an underlying current, or in the understanding of free-surface disturbances induced by vortex and sink flows. Authors who have employed singularities to model underlying flows include Tuck & Vanden-Broeck (1984), Vanden-Broeck & Keller (1987), Mekias & Vanden-Broeck (1989, 1991), Tyvand (1991, 1992), Hocking & Forbes (1992), Miloh & Tyvand (1993), Barnes *et al.* (1996), Xue & Yue (1998), Moreira (2001), Stokes, Hocking & Forbes (2003) and Moreira & Peregrine (2010).

In this work the underlying current is modelled by a distribution of singularities – vortices, sinks and sources – located beneath the free surface, which can induce varied surface current profiles, each of them with a certain minimum and maximum velocity and with a gentle or sharp current gradient. The current is designed to be essentially uniform over the depth of penetration of the wave disturbances but variable in the x-direction. Several singularity distributions were tested based on the experimental current profiles presented by Chawla & Kirby (2002) and Suastika & Battjes (2009). (Actually the present work was motivated by the experimental work first published by Chawla & Kirby 1998 and Suastika *et al.* 2000.)

The chosen singularity distributions satisfy Laplace's equation in the fluid domain and are introduced in our model by decomposing the velocity potential Φ into a regular part ϕ_w(due to surface waves) and a singular part ϕ_s (due to the singularities), such that $\Phi = \phi_w + \phi_s$. To apply Cauchy's integral theorem to the periodic free-surface flow problem, which now includes the singularities, a conformal mapping of the form $\zeta = \mathrm{e}^{-\mathrm{i}z}$ is used, where $z = x + \mathrm{i}y$. No generality is lost in assuming time and space dimensions to be suitably scaled by choosing a certain length to make this period exactly 2π.

For a sharp current gradient, two counter-rotating vortices with strength γ are employed, occupying the positions $z_1(= x_1 + \mathrm{i}y_1)$ and $z_2(= x_2 + \mathrm{i}y_2)$. For deep water, the velocity potential ϕ_s of the flow induced by the pair of point vortices in the ζ-plane is given by (Batchelor 1967)

$$\phi_s(\zeta) = -\gamma \mathrm{Re}\left\{ \mathrm{i} \log\left[\left(\frac{\zeta - \zeta_1}{\zeta - \zeta_2} \right) \left(\frac{\dfrac{1}{\zeta} - \overline{\zeta_2}}{\dfrac{1}{\zeta} - \overline{\zeta_1}} \right) \right] \right\}, \tag{2.4}$$

where $\zeta_1(= \mathrm{e}^{-\mathrm{i}z_1})$ and $\zeta_2(= \mathrm{e}^{-\mathrm{i}z_2})$ represent the corresponding positions of the vortex couple in the ζ-plane; $\overline{\zeta_1}$ and $\overline{\zeta_2}$ are, respectively, the complex conjugates of ζ_1 and ζ_2.

For a gentle surface current gradient, a set of sinks and sources are employed. In the case of a single pair of source and sink, located at ζ_1 and ζ_2 respectively, the velocity potential ϕ_s becomes (Batchelor 1967)

$$\phi_s(\zeta) = \gamma \mathrm{Re}\left\{ \log\left[\left(\frac{\zeta - \zeta_1}{\zeta - \zeta_2} \right) \left(\frac{\dfrac{1}{\zeta} - \overline{\zeta_1}}{\dfrac{1}{\zeta} - \overline{\zeta_2}} \right) \right] \right\}, \tag{2.5}$$

https://doi.org/10.1017/jfm.2011.436 Published online by Cambridge University Press

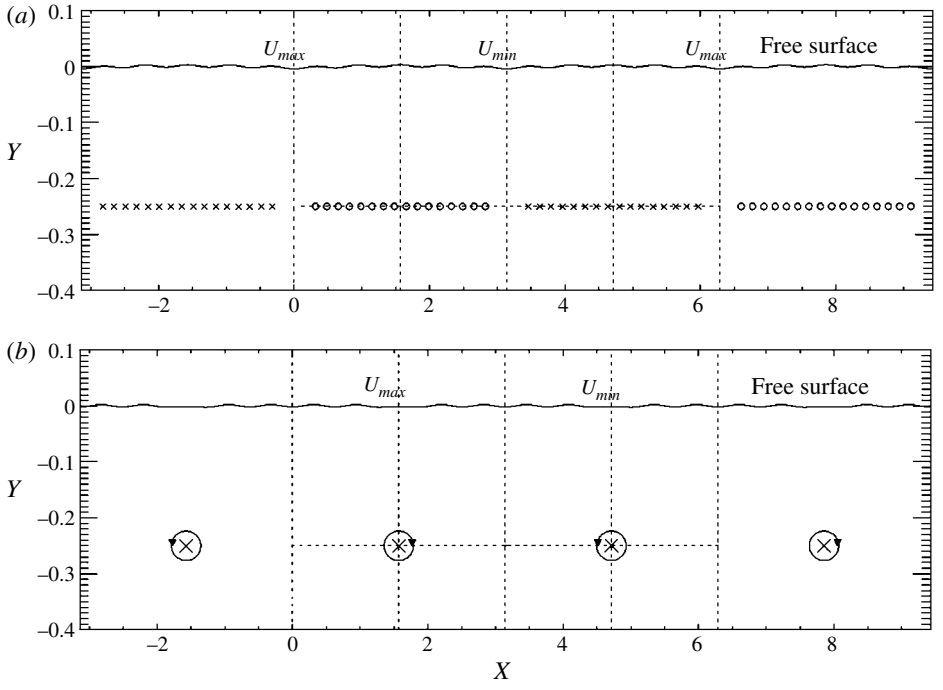


FIGURE 1. A sketch of the fluid domain with an arbitrary free-surface initial condition plus: (*a*) a sink–source distribution (×: sources; ○: sinks); (*b*) an eddy couple.

which is valid for deep water. Here γ is defined as the volume flux per length unit of each of the sinks and sources. Note that the reflection of the singularities onto the free surface, expressed in (2.4) and (2.5), represents a convenient choice for deep water only. They are placed outside the body of the fluid and used to approximate the velocity potential within the fluid. For an unbounded domain with a bed, a vertically periodic set of singularities reflected onto the bed is more appropriate.

The singularities are assumed to be at fixed positions in time such that steady surface currents are imposed on the waves. The singularity distribution has to be weak enough to have little or no effect on the waves such that its existence can be considered unimportant. Therefore only free-surface flows with $Fr \leqslant 0.1$ are employed in this work. This condition is particularly relevant when sharp current gradients are considered. Hence the free-surface waves do not affect the singularities in our nonlinear model. Then the velocity potential ϕ_s satisfies a linear equation beneath the free surface.

Figure 1 sketches the periodic fluid domain with a distribution of 16 sinks and 16 sources and an eddy couple, plus an arbitrary free-surface initial condition. The singularity distributions were chosen to define 'slowly' and 'rapidly' varying surface currents conveniently. Different maxima and minima for the velocity profiles – namely U_{max} and U_{min} – can be obtained by simply varying the sink–source volume flux γ and the vortices depth d. The free-surface current profiles used in the nonlinear computations are detailed in § 4, figure 7.

The method of solution consists of solving numerically an integral equation that arises from Cauchy's integral theorem for functions of a complex variable. Φ is known on the surface for each time step; ϕ_s is then subtracted from the surface value

https://doi.org/10.1017/jfm.2011.436 Published online by Cambridge University Press

of Φ such that the remaining surface wave potential ϕ_w, which has no singularities in the fluid domain, can be used with Cauchy's integral theorem to calculate the velocity $\nabla\phi_w$ on the free surface (Dold 1992). The 'total' surface velocity is then given by $\boldsymbol{u} = \nabla\phi_w + \nabla\phi_s$. The surface profile $\boldsymbol{r}$ and the velocity potential Φ are then stepped in time using a truncated Taylor time series truncated at the sixth power. Since in our model the singularities are assumed to be at fixed positions in time, the partial time derivatives of ϕ_s vanish, though the 'total' surface velocity $\boldsymbol{u}$ and its Lagrangian derivatives are affected directly in our model by the presence of the singularities. For more details on the numerical method see Moreira (2001, Section 2.3).

2.3. *Initial condition for the fully nonlinear model*

The impulsive initial motion of the underlying flow generates disturbances at the free surface. Waves may then be formed as a response to this interaction. Eventually these waves reach regions where the surface current is adverse and sufficiently strong to block their group velocity, increasing their wave steepness and leading to wave breaking, and thus making the analysis more difficult. To construct a suitable initial condition, we superimpose a 'quasi-steady' damped nonlinear solution onto an initially uniform wave train with gentle steepness. The resulting initial condition reduces considerably the disturbances generated by the impulsive initial motion and let us investigate more precisely possible nonlinear effects that would arise due to the interaction between the linear wave train and the singularities. A second-order linearized steady solution for the free-surface elevation is derived in order to compare with the 'quasi-steady' damped nonlinear profiles obtained from the numerical scheme, supposing a simple flat free surface as our initial condition.

Under linear theory, it is possible to solve explicitly the problem of a stationary free-surface flow due to a generic distribution of singularities. Laplace's equation is valid for the whole fluid domain, excluding the singular points $\boldsymbol{x}_{s_i}$, while at the vertical boundaries $\nabla\Phi(0, y) = \nabla\Phi(2\pi, y)$ for $-\infty < y \leqslant 0$. As $\boldsymbol{x} \to \boldsymbol{x}_{s_i}$, the 'total' velocity potential Φ approaches the velocity potential ϕ_s due to the singularities. At the free surface the kinematic and dynamic boundary conditions (2.1) take the stationary form

$$\frac{\partial\Phi}{\partial x}\frac{\partial\eta}{\partial x} = \frac{\partial\Phi}{\partial y}, \quad \frac{1}{2}\left[\left(\frac{\partial\Phi}{\partial x}\right)^2 + \left(\frac{\partial\Phi}{\partial y}\right)^2\right] + g\eta = 0, \tag{2.6}$$

both valid on $y = \eta(x)$.

Assuming that the surface waves are sufficiently small, a linearized steady free-surface solution can be approximated by defining the 'total' velocity potential $\Phi(x, \eta)$ and the free-surface profile $\eta(x)$ in terms of the algebraic expansions

$$\Phi(x, \eta) = \epsilon\Phi_1 + \epsilon^2\Phi_2 + \cdots, \quad \eta(x) = \epsilon\eta_1 + \epsilon^2\eta_2 + \cdots, \tag{2.7}$$

in which ϵ is a small parameter; the functions $\eta_i (i = 1, 2, \ldots)$ depend on x, while Φ_i depends on x and η. Substituting these approximations into (2.6) and extracting the ϵ and ϵ^2 terms gives

$$\eta(x) = -\frac{1}{2g}\left(\frac{\partial\phi}{\partial x}\right)^2, \tag{2.8}$$

where, to simplify the notation, Φ_1 and η_2 were replaced by ϕ and η; ϕ denotes the velocity potential ϕ_s due to any submerged distribution of singularities and satisfies Laplace's equation in the fluid domain, while $\nabla\phi(0, y) = \nabla\phi(2\pi, y)$ for $-\infty < y \leqslant 0$.

https://doi.org/10.1017/jfm.2011.436 Published online by Cambridge University Press

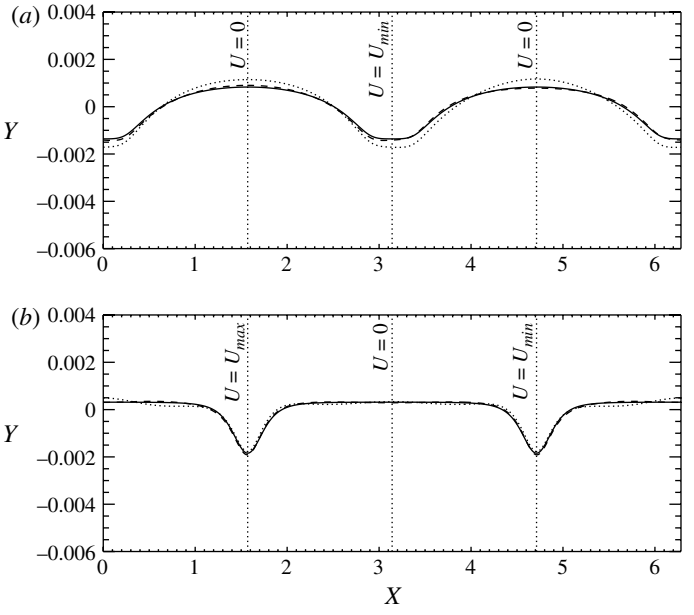


FIGURE 2. The linear steady free-surface solution (——) and the damped nonlinear numerical results due to: (*a*) a distribution of 16 sources and 16 sinks: $Fr = 0.015$, $\delta = 1.5$, $T = 119.0$ (· · · · · ·) and $T = 158.0$ (– – –); (*b*) an eddy couple: $Fr = 0.08$, $\delta = 1.5$, $T = 79.2$ (· · · · · ·) and $T = 119.2$ (– – –). Vertical exaggeration 250:1.

Depending on the magnitude of the surface current induced by the singularities, previous computational runs showed that disturbances generated by the impulsive initial motion at an initially flat free surface may be significant and sufficient to lead to wave breaking. These initial disturbances can be numerically dissipated leading to a 'quasi-steady' surface in finite time. For the purpose of obtaining a suitable initial condition for the fully nonlinear problem, a damping term for the second harmonic of Φ is introduced

$$\Phi(t + \Delta t) = \Phi(t) + \frac{\mathrm{D}\Phi}{\mathrm{D}t}\Delta t + \frac{1}{2}\frac{\mathrm{D}^2\Phi}{\mathrm{D}t^2}\Delta t^2 + \frac{\delta}{2}\frac{\partial^2\Phi}{\partial t^2}\Delta t^2 + O(\Delta t^3), \tag{2.9}$$

where δ is the damping factor.

From now on all the variables in the numerical code are non-dimensionalised such that $X = \kappa x$, $T = t\sqrt{g\kappa}$ and $U = u\sqrt{\kappa/g}$, where κ is the wavenumber; X, T and U are the dimensionless parameters. A comparison between the damped nonlinear results and the linear steady free-surface solutions for a distribution of 16 sinks and 16 sources and an eddy couple is shown in figure 2. Two depressions are formed immediately above the counter-rotating vortices, which approach the linear steady solution given by Novikov (1981); depressions are wider for the sink–source distribution. In both cases, however, the depth of the depression reaches its maximum where the maximum and minimum surface currents are imposed. For bigger Froude numbers these depressions become deeper.

Tests carried out employing the 'stationary' solutions as the initial condition of the numerical code showed that the disturbances generated by the impulsive initial motion have either vanished or appeared in the form of tiny waves with very small amplitude. To include an initially uniform wave train with gentle steepness in our initial condition,

https://doi.org/10.1017/jfm.2011.436 Published online by Cambridge University Press

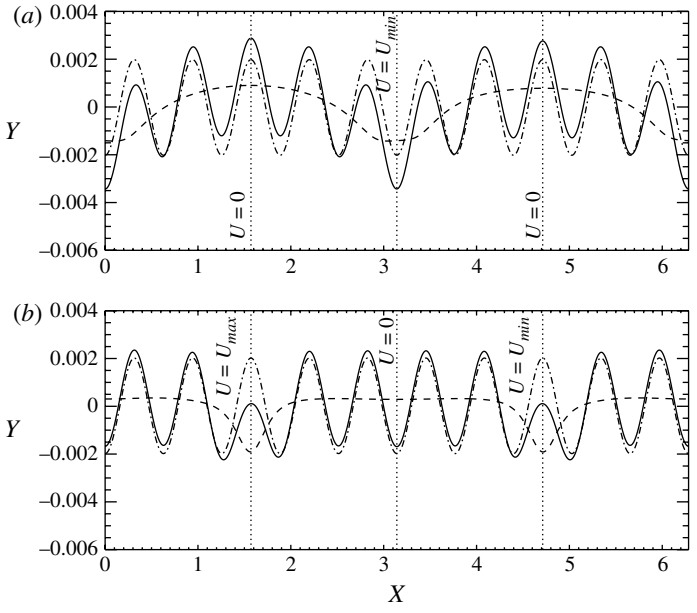


FIGURE 3. The 'stationary' free surface (– – –), the initially uniform wave train with $a_0k_0 = 0.04$ (– · – · –) and the superposition of both profiles (——) due to: (*a*) a distribution of 16 sources and 16 sinks ($Fr = 0.015$); (*b*) an eddy couple ($Fr = 0.08$). a_0 and k_0 represent the wave amplitude and wavenumber at time $T = 0$. Vertical exaggeration 250:1.

we superimpose a train of linear waves onto the 'quasi-steady' solutions obtained. Figure 3 shows the surface elevations, with the solid lines representing the resulting initial conditions. The uniform wave train (dashed–dotted line) follows the 'stationary' solution (dashed line) as its mean level. The same procedure applies to the calculation of the velocity potential.

2.4. *Accuracy of the numerical scheme*

With steep surface phenomena, such as wave breaking, there is a tendency for dramatic changes in properties to take place over relatively small portions of the surface. Nonlinearity exaggerates such changes and thus accuracy may be lost more readily for steep waves than weakly nonlinear waves. Surface resolution may then become relatively poor in regions of high curvature. This lack of resolution occurs when waves are 'about to break' and depends on the 'precision' parameter ε imposed on the nonlinear computations (Dold 1992); ε is used to determine the appropriate stage at which iteration for the potential gradients may cease. It is also employed to specify the convergence of the Taylor series expansion used in the time stepping process. When the free surface contains regions of high curvature or the point distribution becomes too irregular in space, the scheme does not converge and thus the algorithm breaks down. This means that an insufficient number of points could be found if, for example, the wave approaches Stokes' limiting shape (120° at the crest of the calculated wave) or the crest overturns.

Wave breaking is, therefore, very sensitive to the computational parameters. This is demonstrated in figure 4 where three free-surface profiles with different initial discretisations, but with the same accuracy parameter ($\varepsilon = 10^{-6}$) and time ($T = 12.8$), are compared. In this case the initial train of linear water waves did not maintain

https://doi.org/10.1017/jfm.2011.436 Published online by Cambridge University Press

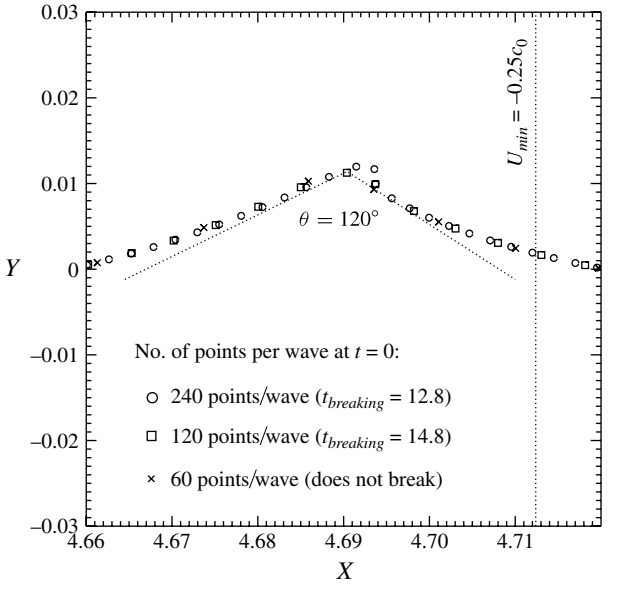


FIGURE 4. Resolution of the surface wave at $T = 12.8$ due to a 'rapidly' varying current ($Fr = 0.08$) for three initially uniform discretisations. The initial train of linear waves has a steepness $a_0k_0 = 0.04$. No vertical exaggeration.

its initial wave form but steepened due to the interaction of an opposing current (for a full discussion see § 4). The more discretisation points that are used, the earlier wave breaking occurs. At low resolutions wave energy is numerically dissipated. Computations are then interrupted as soon as the accuracy required is no longer achieved. For illustration, dotted lines are placed at 120° to each other near the crest of the wave. For an initial discretisation of 120 points per wavelength the computed wave approaches Stokes' limiting shape at $T = 12.8$ and soon wave breaking occurs.

Slightly different surface profiles are also found for regions which contain very short waves on currents if we try to model the same surface with a different number of points. Figure 5 shows the surface profiles obtained from the same starting conditions using 60, 120 and 240 calculation points per wavelength. As already discussed, the difference is most noticeable in the crest of the steepest wave where a high curvature is reached. The reflected waves on the backward face of the steepest wave also present slight differences. The fewer points used, the longer are the reflected waves, with amplitudes decaying quicker with distance from the crest. The decrease in amplitude is attributed to numerical dispersion, which has the effect of smoothing waves with few points per wavelength. To avoid this the computed cases presented here have an initial distribution of 120 points per wavelength, unless otherwise stated. A discussion on the number of points employed to resolve these reflected waves is presented in § 4.1. Sawtooth numerical instabilities were not observed in any of the computations presented in this paper; smoothing was therefore not necessary.

3. Linear wave theory

3.1. *Kinematics of waves on currents*

Most of the theoretical analysis on the interactions between water waves and currents has been developed using linear wave theory. This means that linear results are limited

https://doi.org/10.1017/jfm.2011.436 Published online by Cambridge University Press

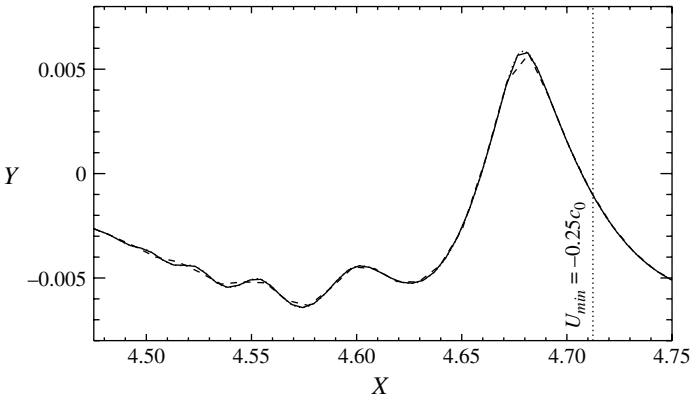


FIGURE 5. Comparison of surface profiles at $T = 10.6$ for an initially uniform discretisation with 60 (– – –), 120 (——) and 240 (· · · · · ·) surface calculation points per wavelength. $Fr = 0.08$, $a_0k_0 = 0.04$. Vertical exaggeration 10:1.

to cases in which changes of the wave properties occur slowly over the wave period. The problem studied here concerns the interaction of periodic waves on a current which varies in the x-direction only i.e. $\boldsymbol{u} = u(x)\boldsymbol{i}$. Only waves travelling directly with or against the current are considered such that $\boldsymbol{k} = k\boldsymbol{i}$. In the absence of surface tension effects and considering that the surface waves propagate in deep water, then the Doppler-shifted dispersion relation simplifies to

$$(\omega - u(x)k)^2 = gk, \tag{3.1}$$

where ω is the wave frequency in a fixed reference frame; $\Omega (= \omega - u(x)k)$ is the wave frequency in a reference frame moving with the current u. The group velocity of the waves relative to the water is then given by $\partial\omega/\partial k$, while the corresponding total group velocity, or total wave energy transport velocity, is defined by $C_g = \partial\Omega/\partial k$.

Figure 6 shows the possible dispersion solutions for opposing and following currents in a one-dimensional flow field. The linear dispersion relation is represented by the solid curve and the Doppler-shifted relation by the straight lines. In the absence of a current, $\Omega = \omega$, and two solution points exist, which correspond to waves moving at a constant phase speed $c = +(g/k)^{1/2}$ if $k > 0$, or $c = -(-g/k)^{1/2}$ if $k < 0$. The relative group velocity $\partial\omega/\partial k$ is the slope of the solid curve, while the total group velocity $\partial\Omega/\partial k$ is given by the difference between the slope of the solid curve and the straight line. Thus for $\Omega = \omega$, $c_g = \pm c/2$, which corresponds to the group velocity for waves in deep water.

In the presence of a current u, with $\Omega = \omega - uk$ and $u_s < u < 0$ (where u_s is the blocking current), four solutions are possible for a fixed wave frequency ω. If k is positive then the current is opposing the wave propagation. The solution point A on figure 6 represents waves with a shorter wavelength (larger wavenumber) compared to the solution without any current. From the graph, it is clear that the total group velocity decreases due to the opposing current, but still $\partial\Omega/\partial k > 0$ for root A. Even though waves are moving against the current, their energy is 'washed down' by the current. If the waves are pushed further into weaker currents, which essentially depends on the sign of $\partial u/\partial x$, their wavelengths keep decreasing. The second solution, given by root B, has waves with very short wavelengths with $\partial\Omega/\partial k < 0$. Reflected waves must then be generated upstream whereas wave energy is swept downstream.

https://doi.org/10.1017/jfm.2011.436 Published online by Cambridge University Press

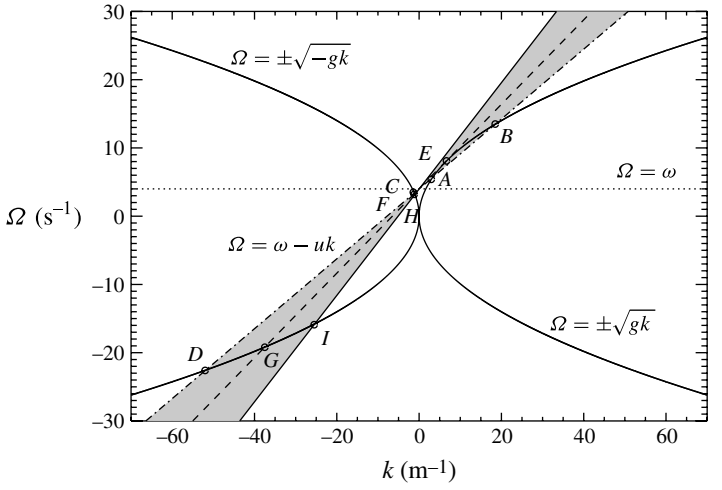


FIGURE 6. Linear dispersion relation (———) and possible dispersion solutions in deep water for $u = 0$ (· · · · · ·), $u_s < u < 0$ (– · – · –), $u = u_s$ (– – –), $u < u_s$ (– · · · – · · · –); u_s is the blocking current. The shaded area represents the region where nonlinear effects are investigated.

The other two solutions, namely C and D, correspond to cases in which waves and current move in the same direction i.e. $k < 0$ and $u_s < u < 0$. It is directly seen from figure 6 (solution point C) that, in comparison with the waves without a current, a following current lengthens the wave instead of shortening it as occurs at point A. This means that the relative phase speed is now augmented by the following current. Root D appears when the Doppler-shifted line crosses the negative branch of the linear dispersion relation. This solution corresponds to very short waves, with both wave crests and energy being swept downstream. Note that for $u > 0$, analogous solutions can be obtained; in this case blocking can only occur if $k < 0$.

The two roots A and B tend to coalesce if the waves propagate into regions of stronger currents, giving in the limiting case a single solution E, which represents the blocking point where $u = u_s$. At this stage the Doppler-shifted line is tangent to the linear dispersion relation and, therefore, $\partial\Omega/\partial k = 0$. The kinematic condition for wave blocking is then satisfied and linear theory becomes singular. The velocity at which the waves' group velocity relative to the water is equal and opposite to the current is known as the stopping velocity where

$$u_s = -\frac{g}{4\omega}. \tag{3.2}$$

The Doppler-shifted line also crosses the dispersion relation at two more solution points, namely F and G. In this case the current follows the wave propagation since $k < 0$ and $u = u_s < 0$. Since the current had increased in magnitude, roots F and G have longer wavelengths when compared to C and D respectively. For stronger currents ($u < u_s$), only two solutions exist for the wave, namely H and I, which are swept downstream. In this case there is no linear solution if $k > 0$. If ω decreases, c_g increases at the blocking point. Thus stronger currents are necessary to block longer waves.

The influence of wave amplitude on the dispersion relation is neglected by linear theory. Stokes was the first to show that this dependence produces important

https://doi.org/10.1017/jfm.2011.436 Published online by Cambridge University Press

qualitative changes in the behaviour of water waves, especially when nonlinear effects arise. The effects of wave amplitude on the dispersion relation when waves are near the blocking point were considered by Longuet-Higgins (1975) and Peregrine & Thomas (1979). They found that the total group velocity $\partial\Omega/\partial k$ in which blocking occurs is greater for the nonlinear case. This means that a stronger free-surface current is then necessary to block the nonlinear waves. The concept of group velocity is very valuable in understanding and predicting the propagation of linear waves. However its extension to nonlinear waves presents difficulties since there are several different velocities which might correspond to a group velocity. Peregrine & Thomas (1979) presented various possible extensions of this concept to nonlinear waves showing the difficulties associated with deep-water waves blocked by an adverse stream.

3.2. *Linear ray theory*

We also use ray theory to model the interaction of the short waves with the surface current due to the singularity distribution. Ray theory assumes that at any particular point the solution surface locally looks like a periodic plane wave train and that any variations in the wave amplitude, frequency and wavenumber are slow, i.e. changes over one wavelength are small. The hypothesis of slow variation of wave properties leads to equations which define lines parallel to the total group velocity of the waves, known as rays. These rays represent a single set of characteristic directions which in one dimension simplifies to

$$\frac{\mathrm{d}x}{\mathrm{d}t} = C_g = u(x) + c_g, \tag{3.3}$$

where $c_g(= c/2)$ is the group velocity for waves in deep water. For a steady surface current the frequency ω is constant along a ray.

Assuming that initially the waves propagate in the positive direction with a phase velocity $c = \sqrt{g/k}$ then the Doppler-shifted dispersion relation (3.1) can be rewritten as

$$\omega c^2 - gc - gu(x) = 0, \tag{3.4}$$

which is a quadratic determining the phase velocity c as a function of the surface current $u(x)$ and the frequency ω. Equation (3.4) gives two solutions for c:

$$c = \frac{g}{2\omega}\left(1 \pm \sqrt{1 + \frac{4\omega u(x)}{g}}\right). \tag{3.5}$$

Thus for a particular ray the quadratic (3.4) defines the frequency ω:

$$\omega = g\left(\frac{1}{c_1} + \frac{u(x_0)}{c_1^2}\right), \tag{3.6}$$

where x_0 is the position of the ray at time $t = 0$ and c_1 is the corresponding value of the phase velocity at that point. Substituting expression (3.6) into (3.5) gives

$$c = \frac{1}{2}\frac{c_1^2}{u(x_0) + c_1}\left[1 \pm \sqrt{1 + 4u(x)\frac{u(x_0) + c_1}{c_1^2}}\right]. \tag{3.7}$$

Restricting the initial conditions to the case with a positive sign (i.e. waves travelling in the same direction as the current), for time $t = 0$, $x = x_0$, and then

https://doi.org/10.1017/jfm.2011.436 Published online by Cambridge University Press

the ray equation (3.3) assumes the form

$$\frac{\mathrm{d}x}{\mathrm{d}t} = u(x_0) + \frac{1}{2}c_1. \tag{3.8}$$

Expression (3.8) determines which root of c should be taken. If in the subsequent propagation of a ray $\mathrm{d}x/\mathrm{d}t = 0$ then the wave is blocked by the current, followed by reflection with respect to the (x, t)-plane. This corresponds to a transfer to the negative root of expression (3.7) for c. Thus energy cannot propagate beyond the blocking point and builds up along the caustic formed. Linear ray theory breaks down near the caustic and either nonlinear effects take over followed possibly by wave breaking, or a uniform solution is needed. The ray diagrams presented in the following section are obtained by integrating expression (3.8) with respect to x and t, and non-dimensionalised as shown in § 2.3.

An expression for the wavenumber $k(=g/c^2)$ can be derived in terms of the surface current $u(x)$ and $u(x_0)$, and the phase velocity c_1. From expression (3.7),

$$k = \frac{4g}{c_1^4}\left[\frac{u(x_0) + c_1}{1 \pm \sqrt{1 + 4u(x)\left[u(x_0) + c_1\right]/c_1^2}}\right]^2. \tag{3.9}$$

Wave amplitudes can also be estimated; for a steady one-dimensional flow, the conservation of wave action equation simplifies to (Bretherton & Garrett 1968)

$$\frac{\partial}{\partial x}\left(C_g \frac{E}{\Omega}\right) = 0. \tag{3.10}$$

The total group velocity C_g is given by expression (3.3) while the wave action E/Ω is defined as

$$\frac{E}{\Omega} = \frac{\rho c a^2}{2}, \tag{3.11}$$

where a is the wave amplitude. Substituting expressions (3.3) and (3.11) into (3.10) and integrating results leads to

$$\frac{a}{a_0} = \sqrt{\frac{c_0^2}{c[c + 2u(x)]}}, \tag{3.12}$$

where a_0 and c_0 are, respectively, the amplitude and the phase velocity at time $t = 0$; and c is given by expression (3.7). For comparison purposes, expressions (3.9) and (3.12) are plotted against the fully nonlinear results in § 4.1, figure 12.

In the light of linear ray analysis it is also possible to estimate the opposing current $u(x)$ necessary to block the incident waves. By substituting the wave frequency ω given by (3.6) into expression (3.2),

$$u_s = -\frac{1}{4}\frac{c_1^2}{u(x_0) + c_1}. \tag{3.13}$$

If $u = u_s$ then, by simple substitution into expressions (3.7) and (3.3), $C_g = 0$, which is exactly the condition for a stopping velocity. For comparison purposes, u_s is non-dimensionalised as in § 2.3 such that $U_s = u_s\sqrt{\kappa/g}$.

https://doi.org/10.1017/jfm.2011.436 Published online by Cambridge University Press

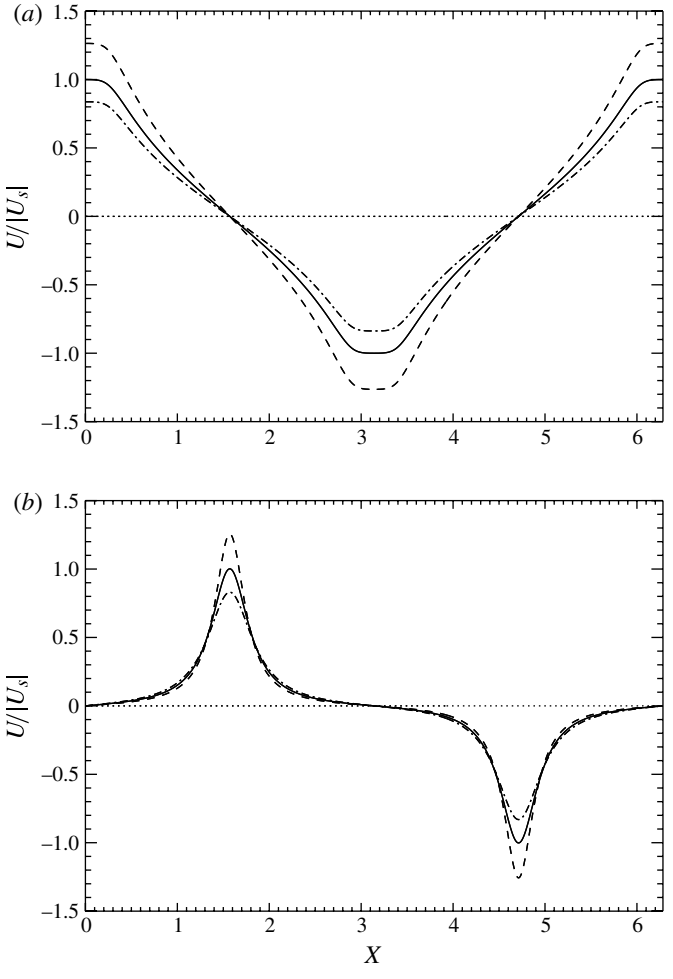


FIGURE 7. Free-surface current profiles induced by: (*a*) 16 sources and 16 sinks ('near-linear' current); (*b*) an eddy couple ('rapidly' varying current). For each case, three peak velocities are considered: $|U_{min}|/|U_s| = |U_{max}|/|U_s| = 1.26$ (— — —); 1.0 (———); 0.83 (—·—·—·).

4. Fully nonlinear results

The nonlinear results consider as an initial condition a set of short waves with initial gentle steepness (set up as explained in § 2.3) interacting with gentle or sharp current gradients, each of them with different peak velocities. Free-surface currents were conveniently chosen such that their minimum velocity U_{min} approaches the stopping velocity U_s of the free-surface waves under still-water conditions. This situation is of especial interest since linear solutions become singular at the blocking point. Figure 7 shows the free-surface current profiles employed in the nonlinear computations. For convenience velocities are expressed in terms of the stopping velocity U_s. Thus three particular situations are of interest and herein studied: $U_{min} < U_s$, $U_{min} = U_s$ and $U_s < U_{min} < 0$, similarly as discussed in § 3.1, figure 6.

Ten initially uniform waves with gentle steepness propagating from the left to the right side are introduced in the periodic domain. In the case of no surface current,

https://doi.org/10.1017/jfm.2011.436 Published online by Cambridge University Press

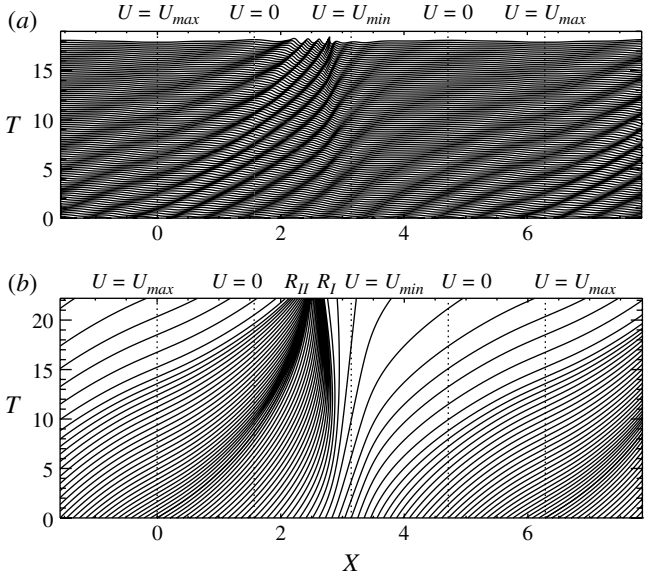


FIGURE 8. Fully nonlinear results (*a*) and the corresponding ray diagram (*b*) due to a 'near-linear' current. $|U_{min}| = |U_{max}| = 1.26|U_s|$, $a_0k_0 = 0.04$, $T_{breaking} = 18.0$.

waves propagate steadily without any distortion since the wave train is too gentle for the Benjamin–Feir instability to develop in the time available. For clarity of the nonlinear results, the stacked free-surface profiles are vertically exaggerated 40 times, unless otherwise stated. As explained in § 3, ray diagrams are also presented for the purpose of comparison. All the computations were done on a Sun Ultra 2/200 with the same accuracy parameters as presented in § 2.4.

4.1. *'Slowly' and 'rapidly' varying surface currents*

Figure 8 shows the stacked free-surface deformation of a wave train with initial gentle steepness $a_0k_0 = 0.04$ and its corresponding ray diagram on the same scale. In this case 16 sinks and 16 sources are symmetrically distributed in the periodic domain at the same depth, imposing a 'near-linear' surface current with $|U_{min}| = |U_{max}| = 1.26|U_s|$ (for details of the surface current profile, see figure 7*a*). The wave transformation that occurs due to the underlying current is clear from figure 8(*a*) . Rough and smooth surfaces can be identified, respectively, downstream and upstream of the U_{min} region after a certain period of time. Some of the waves are steep enough to be noticeably affected by nonlinearity. Rays start to converge as soon as they approach the U_{min} region (see the region indicated by R_I in figure 8*b*), with no focusing occurring in the period of time considered. Associated with R_I, an increase in wave amplitude is observed in the nonlinear calculations, shortly leading to wave breaking with no reflection. Partial wave blocking is predicted by linear ray theory and thus confirmed by the nonlinear computations. There are very few rays upstream of the U_{min} region, exactly where the waves are much less steep with longer wavelengths. Rays also converge in a second region, namely R_{II}, but without wave breaking being seen. Instead, only an increase in wave steepness is associated with R_{II}, which appears from the interaction of rays blocked by U_{min} and rays that had already been accelerated by U_{max}. In fact these two families of rays do overlap at later

https://doi.org/10.1017/jfm.2011.436 Published online by Cambridge University Press

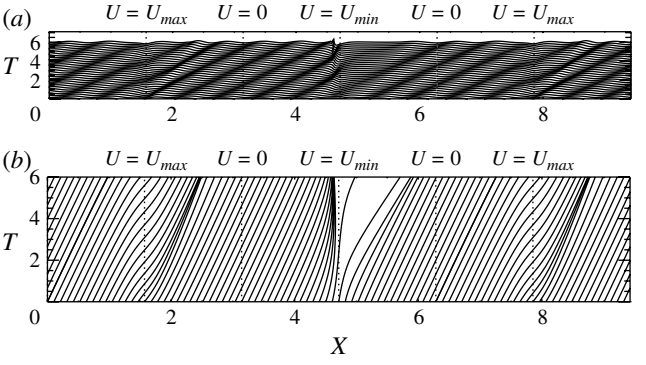


FIGURE 9. Fully nonlinear results (a) and the corresponding ray diagram (b) due to a 'rapidly' varying current. $|U_{min}| = |U_{max}| = 1.26|U_s|$, $a_0k_0 = 0.04$, $T_{breaking} = 6.0$.

times. For the same underlying current, computational runs with gentler initial waves show that, as the initial wave steepness decreases, the corresponding time at which wave breaking occurs increases (e.g. $T_{breaking} = 18.0$ for $a_0k_0 = 0.04$; $T_{breaking} = 21.2$ for $a_0k_0 = 0.02$).

Figure 9 illustrates the free-surface evolution of a similar wave train ($a_0k_0 = 0.04$) and its ray diagram for a 'rapidly' varying surface current. In this case a stationary vortex couple located underneath the free surface induces the same peak velocities $|U_{min}| = |U_{max}| = 1.26|U_s|$ (for details of the surface current profile, see figure 7b). Comparing with the corresponding 'slowly' varying current (see figure 8), waves are blocked sooner with wave breaking occurring three times earlier ($T_{breaking} = 6.0$). It is also possible to notice that for sharp current gradients waves are trapped nearer the U_{min} region. A comparison with the ray diagram shows that rays strongly converge in the region where waves steepen and break. Though this region has a high concentration of rays, no focusing was observed. Since a strong surface current gradient is applied over one wavelength near the U_{min} region, ray theory assumptions are not fully satisfied there, with nonlinear effects taking over. Furthermore, since we are ignoring dissipation, in the linear approximation wave action is conserved in the system as a whole. This implies that wave energy increases for rays moving into regions of greater frequencies and is lost when frequencies decrease. This feature is confirmed by the ray diagram in figure 9(b), where rays are clearly much more spaced upstream of the U_{min} region than downstream.

For weaker currents, figure 10 shows the evolution of short surface waves ($a_0k_0 = 0.04$) interacting with a 'near-linear' current ($|U_{min}| = |U_{max}| = |U_s|$) plus the corresponding ray diagram. The surface current also leads to wave breaking, which now occurs later ($T_{breaking} = 25.4$) and in the region where rays overlap (see figure 10b). When stronger currents are imposed, such as in figure 8, nonlinear effects take over before overlapping occurs; in that case a strong convergence of rays is observed near the U_{min} region. Figure 10(b) also shows a low concentration of rays upstream of the blocking region, with waves much less steep there.

As sharper current gradients are applied, with similar initial conditions ($a_0k_0 = 0.04$) and peak velocities ($|U_{min}| = |U_{max}| = |U_s|$), reflection accompanied by wave breaking appears in the blocking region (see figure 11). This means that part of the wave energy that builds up within the blocking region can be released in the form of partial reflection before wave breaking occurs. This nonlinear feature was not observed when

https://doi.org/10.1017/jfm.2011.436 Published online by Cambridge University Press

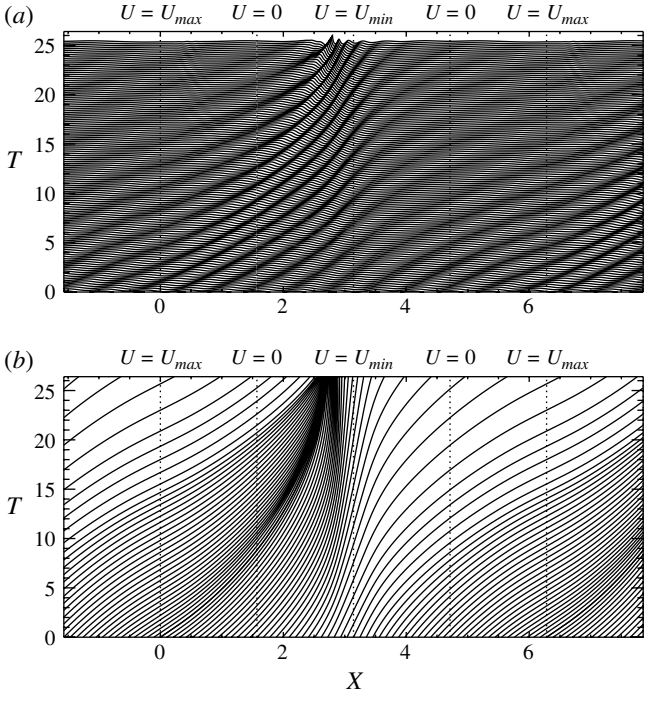


FIGURE 10. Fully nonlinear results (*a*) and the corresponding ray diagram (*b*) due to a 'near-linear' current. $|U_{min}| = |U_{max}| = |U_s|$, $a_0k_0 = 0.04$, $T_{breaking} = 25.4$.

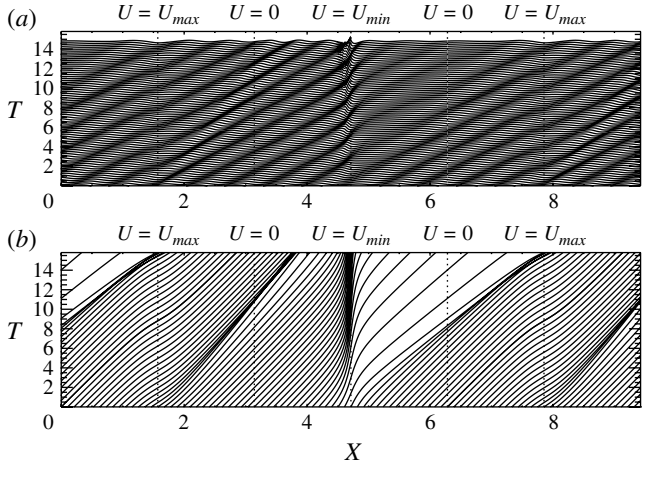


FIGURE 11. Fully nonlinear results (*a*) and the corresponding ray diagram (*b*) due to a 'rapidly' varying surface current. $|U_{min}| = |U_{max}| = |U_s|$, $a_0k_0 = 0.04$, $T_{breaking} = 14.8$.

a 'near-linear' current is applied for similar time (see figure 10). The fully nonlinear results also show that the surface current induced by the eddy couple is sufficient to cause wave steepening and breaking, but still closer to the peak velocity U_{min}. The incident waves are clearly deformed near the maximum and minimum velocity regions,

https://doi.org/10.1017/jfm.2011.436 Published online by Cambridge University Press

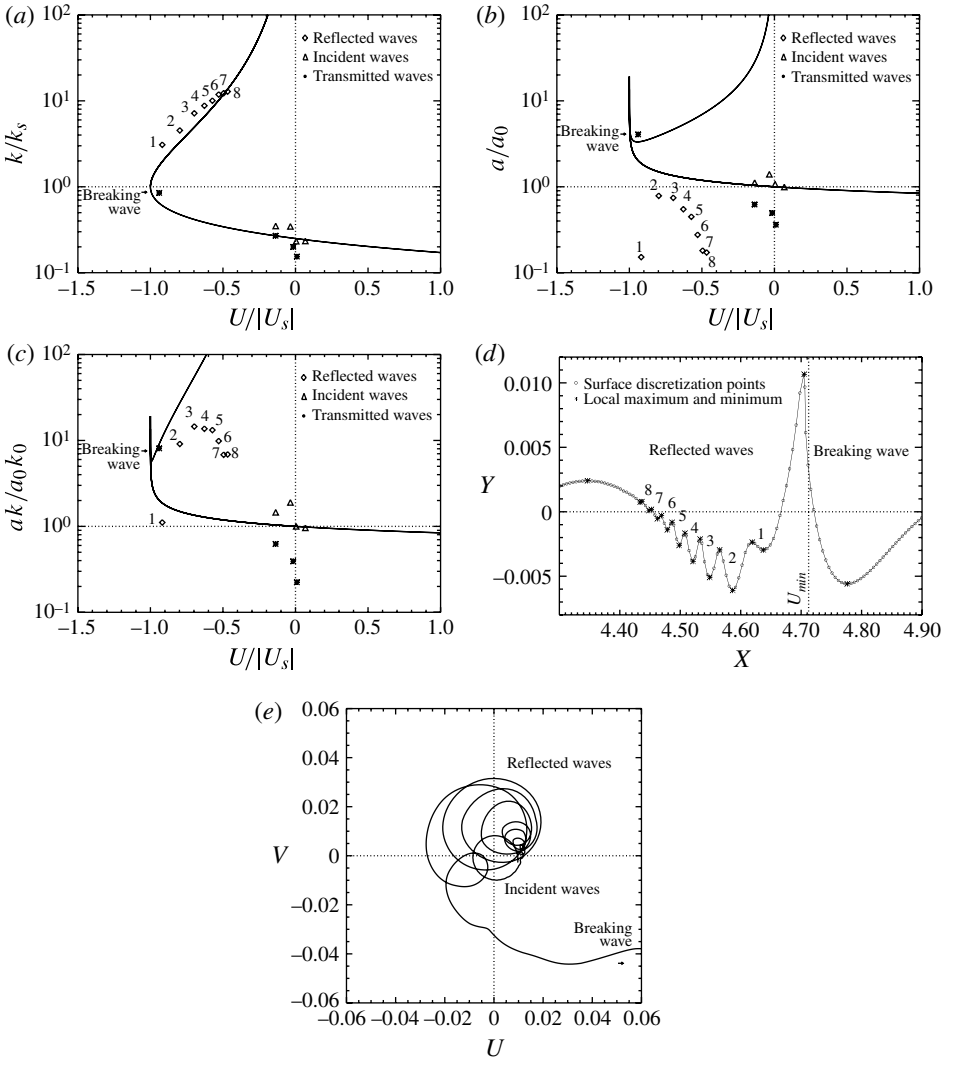


FIGURE 12. Variation of (*a*) wavenumber, (*b*) amplitude, and (*c*) wave steepness, according to linear ray theory (——) and obtained from the fully nonlinear results for a sharp current gradient ($|U_{min}| = |U_{max}| = |U_s|$, $a_0k_0 = 0.04$, $T_{breaking} = 14.8$); (*d*) the reflected waves and (*e*) their corresponding velocities extracted from figure 11(*a*) at the breaking time. Subscript 0 refers to still-water conditions and subscript *s* to conditions at the stopping velocity.

while their group velocity remains unchanged near the regions where $U = 0$. These features are confirmed by the ray diagram in figure 11(*b*), in which rays slow down when passing near the U_{min} region and become more rapid when passing the U_{max} neighbourhood, increasing locally their kinetic energy and group velocity.

Surface wave properties measured from the nonlinear calculations at the breaking time (extracted from figure 11*a*) and from linear ray theory are compared in figure 12. The linear results are evaluated through expressions (3.9) and (3.12) based on the value of the frequency ω of the appropriate ray. From the ray diagram in figure 11(*b*) it is possible to see that this corresponds to a ray initially located in the region where

https://doi.org/10.1017/jfm.2011.436 Published online by Cambridge University Press

a_0k_0	T	Maximum ak/a_0k_0	No. of surface discretisation pts.
	0.00	1.30	107
	3.60	2.20	107
0.04	7.20	5.00	59
	10.8	8.60	30
	14.4	9.80	6
	0.00	1.70	244
	3.60	3.30	138
0.01	7.20	7.60	66
	10.8	10.8	27
	14.4	25.5	6

TABLE 1. Number of surface discretisation points of the steepest waves for $a_0k_0 = 0.04$ and 0.01 propagating over a sharp current gradient ($|U_{min}| = |U_{max}| = |U_s|$) for various times.

the surface current vanishes. Figure 12(*d*) shows the discretisation of the breaking wave, which takes the form of a breaker jet, with the points near the tip tending to move vertically together. Its amplitude is approximately 4 times a_0, the initial wave amplitude (see figure 12*b*). Breaking wave tests carried out by Chawla (1999) also showed that amplitude dispersion plays an important role in determining wave blocking due to the rapid increase in wave steepness close to the blocking point. Because of these substantial amplifications, waves become too steep to be described by an infinitesimal wave theory.

Figure 12(*d*) also shows the discretisation of the reflected waves formed behind the breaking wave. Waves 2 and 3 are particularly well resolved with a minimum of 6 points per wavelength, which represents a reasonable discretisation for gentle waves (Dold 1992). Indeed a comparison between the wavenumbers reveals a good agreement between linear and nonlinear results (see figure 12*a*). A closer look at figures 12(*b*) and 12(*c*) shows that wave steepnesses tend to agree better with ray theory than wave amplitude results. This agreement becomes even better for initially more gentle wave steepnesses, as shown in figure 13. The reflected waves now have a better resolution and thus give better results when compared to linear ray theory. Incident and transmitted waves have their initial resolution practically unchanged. From figures 12(*c*) and 13(*a*) it is possible to verify that incident waves have their steepness increased when on adverse currents, leading to wave breaking close to the stopping velocity, while transmitted waves decrease their steepness substantially, becoming smoother for positive currents. Finally figure 12(*e*) illustrates the corresponding hodograph: the incident linear wave train approaches a circular velocity diagram whereas the reflected waves follow a spiral path with increasingly velocities until breaking occurs.

The validity of the numerical results depends on the resolution of the regions of high curvature. Table 1 shows the resolution of the steepest waves for $a_0k_0 = 0.04$ and 0.01 propagating over a sharp current gradient ($U_{min} = U_s$) at various times. As expected the steepest waves are located near the region where the opposing surface current reaches its maximum. Basically the number of surface discretisation points falls from hundreds to just 6 points per wavelength, which corresponds to the resolution obtained for a reflected wave.

https://doi.org/10.1017/jfm.2011.436 Published online by Cambridge University Press

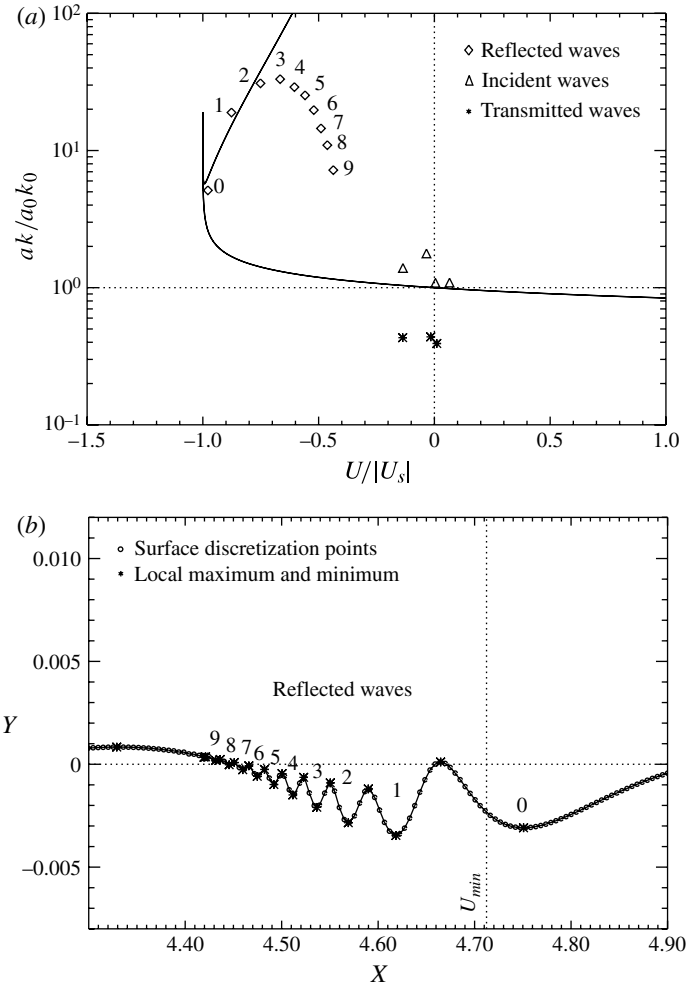


FIGURE 13. Variation of (*a*) wave steepness according to linear ray theory (——) and obtained from the fully nonlinear results for a sharp current gradient ($|U_{min}| = |U_{max}| = |U_s|$, $a_0k_0 = 0.01$, $T_{breaking} = 26.8$); (*b*) the corresponding reflected waves at time $T = 14.8$. Subscript 0 refers to still-water conditions and subscript s to conditions at the stopping velocity.

For weaker currents (e.g. $|U_{min}| = |U_{max}| = 0.83|U_s|$), longer computational runs are needed, which makes the analysis more difficult since the initial waves do not break when crossing the whole period ($0 \leqslant X \leqslant 2\pi$) for the first time. After that, the initial waves have their phase velocity substantially changed by the imposed surface current. Waves get 'steeper' in the U_{min} region with breaking occurring in the region where rays overlap; upstream of the blocking region waves have their steepness reduced. Despite the accumulated changes imposed by weaker currents on the initially uniform wave train along the periodic domain, results show that linear ray theory can still predict the region where wave steepening and breaking occur, with a high convergence of rays and caustics being formed within that region. Indeed, for longer computational runs in a similar spatially periodic domain, Donato *et al.* (1999) also

https://doi.org/10.1017/jfm.2011.436 Published online by Cambridge University Press

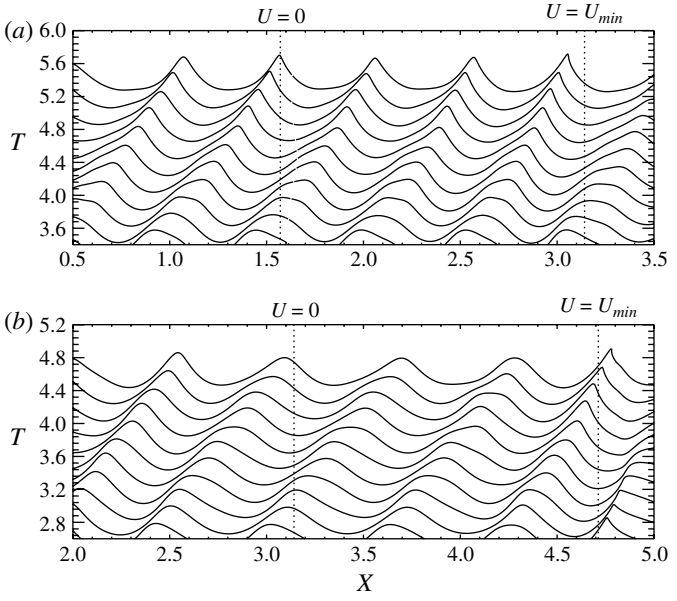


FIGURE 14. Final stages up to wave breaking due to: (*a*) a 'slowly' varying current ($T_{breaking} = 5.4$); (*b*) a 'rapidly' varying current ($T_{breaking} = 4.6$). In both cases $|U_{min}| = |U_{max}| = 0.83|U_s|$, $a_0k_0 = 0.40$. No vertical exaggeration.

found a good agreement between linear ray theory and fully nonlinear results despite all the accumulated changes in the wave pattern.

4.2. *'Steeper' initial conditions and wave breaking*

The effects of underlying currents on waves with greater steepnesses are of interest and also investigated here. Figure 14 shows with no vertical exaggeration the last steps until wave breaking occurs when steep waves ($a_0k_0 = 0.40$) interact with a 'slowly' and a 'rapidly' varying current ($U_{min} = 0.83U_s$). Under these conditions waves are noticeably affected by nonlinearity. However the sink–source distribution causes wave steepening in larger regions than the current induced by the eddy couple. Waves do steepen locally due to the vortex flow in a way sufficient to stop the computations before the 'slowly' varying current case. In both cases the breaking wave takes the form of a breaker jet, approaching Stokes' limiting shape of 120° at the crest, with no overturning being observed. Tanaka (1983) found that regular waves on deep water break when their steepnesses exceed approximately $ak = 0.43$, which corresponds to the maximum value found in the computations. Similar features were also observed for smaller initial wave steepnesses.

Figure 15 shows the time of breaking of short surface waves propagating over the non-uniform currents versus three initial wave steepnesses ($a_0k_0 = 0.04, 0.20, 0.40$) with the same resolution (120 points/wave) and accuracy parameters defined in § 2.4. In general strong 'rapidly' varying currents ($U_{min}/U_s = 1.26,\ 1.0$) induce wave breaking at shorter times than the corresponding 'slowly' varying currents. An exception occurs for weaker currents ($U_{min}/U_s = 0.83$); in this case the sharp current gradient seems to be less effective in causing local wave steepening and breaking. In fact, at a certain instant of time, the total kinetic energy transferred to the surface waves by the 'near-linear' current is greater than the vortex-induced current, which can

https://doi.org/10.1017/jfm.2011.436 Published online by Cambridge University Press

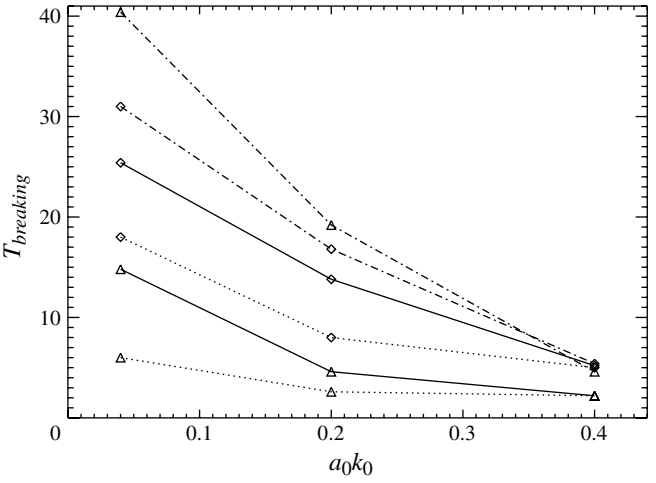


FIGURE 15. Time of breaking against initial wave steepnesses of the surface waves for 'slowly' (◇) and 'rapidly' (△) varying currents, and $|U_{min}| = |U_{max}| = 1.26|U_s|$ (· · · · · ·); $|U_{min}| = |U_{max}| = |U_s|$ (——); $|U_{min}| = |U_{max}| = 0.83|U_s|$ (– · – · –).

explain the shorter breaking times found for this case. The shorter times to breaking occur for all the computed cases when $a_0k_0 = 0.40$, which agrees with the theory that regular waves on deep water break when their steepness exceeds $ak = 0.43$.

4.3. *Wave group interactions*

Finally the numerical scheme was used to simulate the interactions between wave groups and currents. The wave groups were constructed by superposing two monochromatic waves having the same amplitude but slightly different frequencies, with the difference between the frequencies determining the number of waves in a group. This spectral approach was also employed by Chawla (1999). Based on his cleanest wave groups, i.e. bichromatic waves with no energy transferred to the side bands, we set up our initial condition by superposing two uniform wave train components with $a_0k_0 = 0.06$, 0.084 and $k_0 = 10$, 14, respectively. The evolution of these wave groups over 'slowly' and 'rapidly' varying currents is shown in figures 16(*b*) and 16(*c*). For comparison purposes wave groups propagating over still water are presented in figure 16(*a*). These results show that partial wave blocking can occur at the individual wave components in the wave groups and that waves become almost monochromatic beyond the U_{min} region, which is clearer from figure 16(*b*). In both cases the numerical computations stop due to wave breaking. For sharp current gradients, wave breaking occurs nearer the U_{min} region, with no reflection being observed for the period of time considered. The modulation of weakly nonlinear water waves is governed by the nonlinear Schrödinger equation. Results of the current-modified nonlinear Schrödinger equation have shown a good agreement with the fully nonlinear boundary-integral solver for a periodic surface current with a small, slow variation from a mean value (Stocker & Peregrine 1999).

5. Summary

The interaction between water waves and currents was investigated numerically with special attention paid to the effects of nonlinearity at the free surface.

https://doi.org/10.1017/jfm.2011.436 Published online by Cambridge University Press

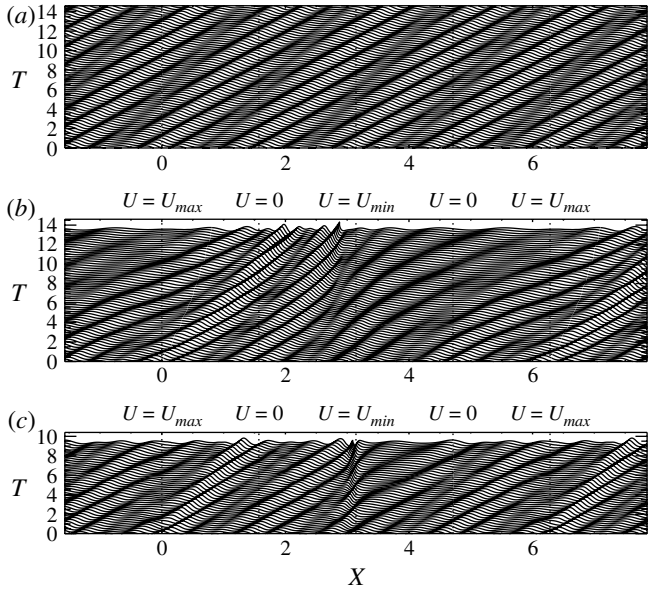


FIGURE 16. Fully nonlinear results obtained for wave groups propagating over (*a*) still water, (*b*) a'slowly' varying current ($|U_{min}| = |U_{max}| = |U_s|$, $T_{breaking} = 13.6$) and (*c*) a 'rapidly' varying current ($|U_{min}| = |U_{max}| = |U_s|$, $T_{breaking} = 9.4$).

A fully nonlinear model was developed in order to understand the interaction of stationary submerged currents induced by singularities with a large number of short surface waves. The nonlinear numerical results show that adverse currents induce wave steepening and breaking. Furthermore the wave transformation induced by the underlying flows can be identified by a steep and a smooth region formed, respectively, downstream and upstream of the U_{min} region after a certain period of time. A strong increase in wave steepness is observed within the blocking region, leading to wave breaking, while wave amplitudes decrease significantly beyond this region. The numerical simulations also show that wave blocking and breaking are more prominent for sharp surface current gradients. For these cases the nonlinear wave properties reveal that reflection does occur near the U_{min} region for sufficiently strong adverse currents, thus confirming that at least some of the wave energy that builds up within the caustic can be released in the form of partial reflection (which applies to very gentle waves) and wave breaking (even for small-amplitude waves). For 'steeper' initial conditions, e.g. $a_0k_0 = 0.40$, wave breaking occurs much earlier, with no reflection being observed and with the breaking wave approaching Stokes' limiting shape. In the case of interactions between wave groups and currents, nonlinear results show that wave blocking can occur for the individual wave components in the wave groups and that waves evolve from being in groups to being almost monochromatic, confirming qualitatively the experimental observations of Chawla (1999).

Acknowledgements

R.M.M. acknowledges the financial support through CAPES, the Brazilian agency for postgraduate education, and CNPq, the national research and development council (contract number 62.0018/2003-8- PADCT III/FAPERJ); and is grateful for

https://doi.org/10.1017/jfm.2011.436 Published online by Cambridge University Press

the referees' comments and also for discussions carried out with Dr A. Chawla, Dr I. K. Suastika, Dr J. R. Stocker and Dr J. T. A. Chacaltana. This paper is dedicated to the memory of Dr A. F. Teles da Silva.

REFERENCES

BARNES, T. C. D., BROCCHINI, M., PEREGRINE, D. H. & STANSBY, P. K. 1996 Modelling post-wave breaking turbulence and vorticity. In *Proceedings of the 25th International Conference on Coastal Engineering*, pp. 186–199. ASCE.

BATCHELOR, G. K. 1967 *An Introduction to Fluid Dynamics*. Cambridge University Press.

BATTJES, J. A. 1982 A case study of wave height variations due to currents in a tidal entrance. *Coast. Engng* **6**, 47–57.

BRETHERTON, F. P. & GARRETT, C. J. R. 1968 Wavetrains in inhomogenous moving media. *Proc. R. Soc. Lond.* A **302**, 529–554.

CHAWLA, A. 1999 An experimental study on the dynamics of wave blocking and breaking on opposing currents. PhD thesis, University of Delaware, USA.

CHAWLA, A. & KIRBY, J. T. 1998 Experimental study of wave breaking and blocking on opposing currents. In *Proceedings of the 26th International Conference on Coastal Engineering*, pp. 759–772. ASCE.

CHAWLA, A. & KIRBY, J. T. 2002 Monochromatic and random wave breaking at blocking points. *J. Geophys. Res.* **107** (C7), doi:10.1029/2001JC001042.

CHEN, Q., MADSEN, P. A., SCHÄFFER, H. A. & BASCO, D. R. 1998 Wave-current interaction based on an enhanced Boussinesq approach. *Coast. Engng* **33**, 11–39.

CRAPPER, G. D. 1972 Nonlinear gravity waves on steady non-uniform currents. *J. Fluid Mech.* **52**, 713–724.

DOLD, J. W. 1992 An efficient surface-integral algorithm applied to unsteady gravity waves. *J. Comput. Phys.* **103**, 90–115.

DOLD, J. W. & PEREGRINE, D. H. 1986 An efficient boundary-integral method for steep unsteady water waves. In *Numerical Methods for Fluid Dynamics II* (ed. K. W. Morton & M. J. Baines), pp. 671–679. Oxford University Press.

DONATO, A. N., PEREGRINE, D. H. & STOCKER, J. R. 1999 The focusing of surface waves by internal waves. *J. Fluid Mech.* **384**, 27–58.

HOCKING, G. C. & FORBES, L. K. 1992 Subcritical free-surface flow caused by a line source in a fluid of finite depth. *J. Engng Maths* **26**, 455–466.

JONSSON, I. G. 1990 Wave-current interactions. In *The Sea: Ocean Engineering Science 9A* (ed. B. Le Mehaute & D. M. Hanes), pp. 65–120. Wiley Interscience.

KHARIF, C. & PELINOVSKY, E. 2006 Freak waves phenomenon: physical mechanisms and modelling. In *Waves in Geophysical Fluids: CISM Courses and Lectures 489* (ed. J. Grue & K. Trulsen), pp. 107–172. Springer.

LAI, R. J., LONG, S. R. & HUANG, N. E. 1989 Laboratory studies of wave-current interaction: kinematics of the strong interaction. *J. Geophys. Res.* **94**, 16201–16214.

LAMB, H. 1932 *Hydrodynamics*. Cambridge University Press.

LONGUET-HIGGINS, M. S. 1975 Integral properties of periodic gravity waves of finite amplitude. *Proc. R. Soc. Lond.* A **342**, 157–174.

LONGUET-HIGGINS, M. S. & STEWART, R. W. 1960 Changes in the form of short gravity waves on long waves and tidal currents. *J. Fluid Mech.* **8**, 565–583.

LONGUET-HIGGINS, M. S. & STEWART, R. W. 1961 The changes in amplitude of short gravity waves on non-uniform currents. *J. Fluid Mech.* **10**, 529–549.

MALLORY, J. K. 1974 Abnormal waves in the south-east coast of South Africa. *Intl Hydrog. Rev.* **51**, 99–129.

MEKIAS, H. & VANDEN-BROECK, J.-M. 1989 Supercritical free-surface flow with a stagnation point due to a submerged source. *Phys. Fluids* A **1**, 1694–1697.

MEKIAS, H. & VANDEN-BROECK, J.-M. 1991 Subcritical flow with a stagnation point due to a source beneath a free surface. *Phys. Fluids* A **3**, 2652–2658.

https://doi.org/10.1017/jfm.2011.436 Published online by Cambridge University Press

MILOH, T. & TYVAND, P. A. 1993 Nonlinear transient free-surface flow and dip formation due to a point sink. *Phys. Fluids* A **5**, 1368–1375.

MOREIRA, R. M. 2001 Nonlinear interactions between water waves, free-surface flows and singularities. PhD thesis, University of Bristol, UK.

MOREIRA, R. M. & PEREGRINE, D. H. 2010 Nonlinear interactions between a free-surface flow with surface tension and a submerged cylinder. *J. Fluid Mech.* **648**, 485–507.

NOVIKOV, YE. A. 1981 Generation of surface waves by discrete vortices. *Izv. Atmos. Ocean. Phys.* **17**, 709–714.

PEREGRINE, D. H. 1976 Interaction of water waves and currents. *Adv. Appl. Mech.* **16**, 9–117.

PEREGRINE, D. H. & SMITH, R. 1979 Nonlinear effects upon waves near caustics. *Phil. Trans. R. Soc. Lond.* A **292**, 341–370.

PEREGRINE, D. H. & THOMAS, G. P. 1979 Finite-amplitude deep-water waves on currents. *Phil. Trans. R. Soc. Lond.* A **292**, 371–390.

RIS, R. C. & HOLTHUIJSEN, L. H. 1996 Spectral modelling of current induced wave-blocking. In *Proceedings 25th International Conference on Coastal Engineering*, pp. 1246–1254. ASCE.

SAKAI, S. & SAEKI, H. 1984 Effects of opposing current on wave transformation. In *Proceedings 19th International Conference on Coastal Engineering*, pp. 1132–1148. ASCE.

SMITH, R. 1975 The reflection of short gravity waves on a non-uniform current. *Proc. Camb. Phil. Soc.* **78**, 517–525.

STIASSNIE, M. & DAGAN, G. 1979 Partial reflexion of water waves by non-uniform adverse currents. *J. Fluid Mech.* **92**, 119–129.

STOCKER, J. R. & PEREGRINE, D. H. 1999 The current-modified nonlinear Schrödinger equation. *J. Fluid Mech.* **399**, 335–353.

STOKES, T. E., HOCKING, G. C. & FORBES, L. K. 2003 Unsteady free-surface flow induced by a line sink. *J. Engng Maths* **47**, 137–160.

SUASTIKA, I. K. & BATTJES, J. 2009 A model for blocking of periodic waves. *Coast. Engng J.* **51**, 81–99.

SUASTIKA, I. K., DE JONG, M. P. C. & BATTJES, J. A. 2000 Experimental study of wave blocking. In *Proceedings 27th International Conference on Coastal Engineering*, pp. 223–240. ASCE.

TANAKA, M. 1983 The stability of steep gravity waves. *J. Phys. Soc. Japan* **52**, 3047–3055.

THOMAS, G. P. & KLOPMAN, G. 1997 Wave-current interactions in the nearshore region. In *Gravity Waves in Water of Finite Depth* (ed. J.N. Hunt), pp. 215–319. Computational Mechanics Publications.

TUCK, E. O. & VANDEN-BROECK, J.-M. 1984 A cusplike free-surface flow due to a submerged source or sink. *J. Austral. Math. Soc.* B **25**, 443–450.

TYVAND, P. A. 1991 Motion of a vortex near a free surface. *J. Fluid Mech.* **225**, 673–686.

TYVAND, P. A. 1992 Unsteady free-surface flow due to a line source. *Phys. Fluids* A **4**, 671–676.

VANDEN-BROECK, J.-M. & KELLER, J. B. 1987 Free surface flow due to a sink. *J. Fluid Mech.* **175**, 109–117.

VINCENT, C. E. 1979 The interaction of wind-generated sea waves with tidal currents. *J. Phys. Oceanogr.* **9**, 748–755.

XUE, M. & YUE, D. K. P. 1998 Nonlinear free-surface flow due to an impulsively-started submerged point sink. *J. Fluid Mech.* **364**, 325–347.

https://doi.org/10.1017/jfm.2011.436 Published online by Cambridge University Press